Prediction of crack initiation at blunt notches and cavities – size effects

Dominique Leguillon, Daniel Quesada, Claude Putot, Eric Martin

Prediction of crack initiation at blunt notches and cavities – size effects

D. Leguillon [a,*], D. Quesada [a,b], C. Putot [b], E. Martin [c]

[a] *LMM, CNRS UMR 7607, Université P. et M. Curie, Paris, France*
[b] *IFP, Direction Mécanique Appliquée, Rueil Malmaison, France*
[c] *LCTS, CNRS UMR 5801, Université Bordeaux 1, Pessac, France*

Crack initiation at corners, V-notches and other situations such as interfaces breaking a free surface (delamination initiation) cannot be correctly predicted by the usual brittle fracture criteria (either Griffith or maximum stress). They give contradictory results and neither one nor the other agrees with the experiments. An additional characteristic length is required to define a satisfying criterion giving rise to the so-called "Finite fracture mechanics". The crack is supposed to jump this length which depends both on the material properties and the local geometry of the structure; it is not a mate-rial parameter. In most cases this crack increment is small. The size effect arises with the interaction between the crack increment and another length characterising a microstructure such as a pore diameter, a notch root radius or an interface layer thickness. The remote load at failure depends on the actual value of this microstructure parameter whereas it was not expected in all cases. Assuming that the two interacting lengths remain small compared to the size of the global structure, an asymptotic procedure allows bringing into evidence the change in the apparent resistance of the structure due to this phenomenon. Results are compared with experiments in various domains: polymers, ceramics and rocks.

Keywords: Fracture mechanics; Crack initiation; Size effects

1. Introduction

Experiments carried out on specimens under uniaxial tensile or compressive load mainly show a dependency of material performances on the various characteristic lengths involved at each scale of study in the material, termed size effect. The load at failure, for instance, decreases with the size or volume of the specimen. Weibull developed in 1939 [1] a theory, based on the weakest link concept, demonstrating the existence of a so-called statistical size effect, which can be synthesized as follows: the larger the specimen, the higher the

* Corresponding author. Address: LMM, University Paris 6, Case 162, 4 Place Jussieu, 75252 Paris Cedex 05, France. Tel.: +33 1 44 27 53 22; fax: +33 1 44 27 52 59.
E-mail address: dol@ccr.jussieu.fr (D. Leguillon).

Nomenclature

a	sediments bed thickness (m)
A, B, D	scaling coefficients (MPa^{-1})
d	characteristic length of the microstructure (m)
e	specimens or structures thickness (plane elasticity) (m)
$E, E_\mathrm{i}, C, v, v_\mathrm{i}$	Young's moduli, stiffness matrix (MPa) and Poisson's ratios
G_c	toughness ($\mathrm{J\,m}^{-2}$)
$G_\mathrm{i}, G_\mathrm{d}$	incremental and differential energy release rates ($\mathrm{J\,m}^{-2}$)
$F_\mathrm{i}, H_\mathrm{i}$	Gauge functions of the inner expansions
k_I	Mode I stress intensity factor ($\mathrm{MPa\,m}^{1/2}$)
$k_{I\mathrm{c}}, k_{I\mathrm{c}}^{\mathrm{app}}$	toughness and apparent toughness ($\mathrm{MPa\,m}^{1/2}$)
k	generalized stress intensity factor, GSIF ($\mathrm{MPa\,m}^{1-\lambda}$)
$k_\mathrm{c}, k_\mathrm{c}^{\mathrm{app}}$	critical GSIF and apparent critical GSIF ($\mathrm{MPa\,m}^{1-\lambda}$)
ℓ, ℓ_0	crack increment length (generic and at initiation) (m)
$\underline{n}, \underline{N}$	unit normal vectors
T	uniform tension (MPa)
R	ratio of the apparent critical GSIF to the critical GSIF
$\underline{U}$	generic elastic displacement field (m)
$\underline{U}^\ell, \underline{U}^{\ell,d}$	actual elastic solutions (m)
$\underline{U}^0$	leading term of the outer expansion, far field (m)
$\underline{u}_I, \underline{u}, \underline{u}^-, \underline{t}$	angular shape functions associated with the exponents 1/2, λ, $-\lambda$ and 1 (MPa^{-1})
$\underline{V}^\mathrm{i}, \underline{\widehat{V}}^\mathrm{i}, \underline{W}^\mathrm{i}$	terms of the inner expansions, near field (MPa^{-1})
x_1, x_2, r, θ	physical Cartesian and polar coordinates
$y_1, y_2, y_1', y_2', \rho, \theta, \rho'$	stretched dimensionless coordinates
δS	newly created crack surface (m^2)
$\delta W_\mathrm{p}, \delta W_\mathrm{k}$	change in potential and kinetic energy (J)
Γ_∞	artificial boundary in the inner domain
λ	singularity exponent
μ, μ_0	stretched crack lengths (generic and at initiation)
σ	tension orthogonal to the failure direction (MPa)
σ_c	tensile strength (MPa)
$\underline{\underline{\sigma}}$	stress tensor with components $\sigma_{11}, \sigma_{12}, \sigma_{22}$ or $\sigma_{rr}, \sigma_{r\theta}, \sigma_{\theta\theta}$ (MPa)
$\underline{\underline{\tilde{\sigma}}}$	stress tensor with components $\tilde{\sigma}_{11}, \tilde{\sigma}_{12}, \tilde{\sigma}_{22}$ in the stretched domain
σ^∞, κ	remote load (MPa) and unitary GSIF ($\mathrm{m}^{1-\lambda}$)
Ψ	path independent integral
ω	V-notch opening (°)
$\nabla_x^\mathrm{S}, \nabla_y^\mathrm{S}$	symmetric part of the gradient with respect to x (resp. to y)

probability of presence of a big defect leading to a lower resistance. This result, built rather on a probabilistic background than on a true mechanical formulation, can somehow explain some size effects observed in specimens under traction, but appears to be far less relevant when the specimens are submitted to compressive loads. Indeed, macroscopic crack propagation, in materials such as rocks, occurs in a quite stable way, and the size effect observed then is too important to result only from a statistical size effect, which will therefore not be addressed herein. This consideration has given birth to Bazant's determinist theory [2–4], which proposes a formulation characterizing a so-called fracture mechanics size effect. His model, using a non-linear form of elastic fracture mechanics equations, was applied to and validated in a wide range of situations, among which: fracture in compression [2], tensile fracture in concrete, rocks or metal [3]. According to this theory, the size of the process zone in front of the crack tip (yielding in metals or microfracturing in rocks or concrete) which is a material characteristic depending on the maximum aggregate size is an important

characteristic length of the structure. These materials are baptised quasi-brittle according to the existence of such a damage process zone ahead of the crack tip. For small size specimens, in which the process zone is of wide extent, a strength criterion must be used to predict failure. In contrast, for large size specimens, the size of the process zone becomes negligible, and the energy criterion of linear fracture mechanics is well adapted to failure prediction. For intermediate sizes, the size effect consists in a smooth transition between the strength criterion for small sizes and energy criterion for large sizes.

Herein we proposed a different approach, coupling finite fracture mechanics [5–7] with a characteristic size of the microstructure, to analyse crack nucleation in brittle materials at stress concentration points. One of the authors showed, in a previous paper [8], that an additional characteristic length is required to define a satisfying initiation criterion. At onset the crack is supposed to jump this length which depends both on the material properties and the local geometry around the stress concentration point, but not on the global size of the structure. This increment is not a material parameter (the local geometry intervenes) and in most cases it is small. The size effect arises with the interaction between the crack increment and another length characterising a microstructure such as a pore diameter, a notch root radius or an interface layer thickness. The remote load at failure depends on the actual value of this microstructure parameter whereas it was not expected in all cases. Assuming that the two interacting lengths remain small compared to the size of the global structure, an asymptotic procedure allows bringing into evidence the influence of this phenomenon on the apparent resistance of the structure. Results are compared with experiments in various domains: polymers, ceramics and rocks.

The reasoning has been applied successfully to blunt notches [9,10], the notch root radius playing the role of the microstructure characteristic length; to cracks impinging on an interlayer, the microstructure length being the interphase thickness. This last case applies to various mechanisms such as the step-over in bedded sediments [11]; the role of an adhesive layer between two steel plates [12]; the crack path in ceramic laminates [13], the interface debonding ahead of a matrix crack [14,15].

The common feature of these situations is the existence at the macro scale (when the microstructure length is neglected) of a singular point [16]. In this paper we extend the results to non-singular situations of stress concentrations. Two problems are analyzed: the crack initiation at a hole in a plate of PMMA under tension, and the crack initiation at a hole in a block of rock under compression. In both, the small parameter characteristic of the microstructure is the diameter of the hole, allowing, as previously done, a matched asymptotics procedure.

Failure of brittle materials under compressive conditions has been a common issue of fracture mechanics for years. Among all the papers on the subject, Sammis and Ashby [17] have developed a theory of damage mechanics for brittle porous materials under compressive stress states, He et al. [18] have carried out a numerical study of the problem, and Wong et al. [19] have conducted an experimental and numerical study on splitting failure of brittle solids containing single pore under uniaxial compression. Comparisons with experiments are performed herein using the work of Li and Zhang [20] for drilled plates of PMMA in traction and that of Carter and Carter et al. [21,22] for holed plates of rocks in compression.

2. Brittle fracture criteria

Brittle fracture mechanics traditionally make use either of the Griffith criterion or of the maximum stress criterion. They are briefly recalled below.

2.1. The energy criterion for fracture

The Griffith criterion is based on an energy balance between an elastic initial state prior to any crack onset or growth and after the appearance of a crack extension of surface δS

$$\delta W_{\mathrm{p}} + \delta W_{\mathrm{k}} + G_{\mathrm{c}}\delta S = 0 \tag{1}$$

where δW_{p} is the change in potential energy, δW_{k} the change in kinetic energy and $G_{\mathrm{c}}\delta S$ the fracture energy (G_{c} is the material toughness (J m^{-2})). The toughness can be also expressed in terms of the critical mode I stress intensity factor k_{Ic} (MPa m$^{1/2}$) using the Irwin relation

$$G_c = \frac{1-\nu^2}{E} k_{Ic}^2 \tag{2}$$

where E and ν are respectively the Young's modulus and the Poisson's ratio of the material. Depending on the experimental data, one or the other parameter will be used in the following.

If the initial state is quasi-static, then there is production of kinetic energy and

$$\delta W_k \geqslant 0 \Rightarrow -\frac{\delta W_p}{\delta S} = G_i \geqslant G_c \text{ (incremental)} \tag{3}$$

It is an unquestionable necessary condition for failure, G_i is the (incremental) energy release rate. The above inequality involves the a priori unknown surface increment δS.

In case of a continuous crack growth, one can derive from the above inequality, by derivation ($\delta S \to 0$), the so-called Griffith criterion

$$-\frac{\partial W_p}{\partial S} = G_d \geqslant G_c \text{ (differential)} \tag{4}$$

Here G_d is the (differential) energy release rate. This final criterion does not involve any length or crack increment. Nevertheless, the existence of the derivative is rarely considered while it deserves a discussion.

2.1.1. Maximum stress criterion

If no pre-existing crack exists the maximum stress criterion is often invoked. It is based on the maximum tension that a material can bear. Failure occurs at a point if

$$\sigma \geqslant \sigma_c \tag{5}$$

where σ holds for the tension orthogonally to the failure direction and σ_c for the tensile strength of the material.

2.1.2. Discussion

Nevertheless, the crack initiation at corners, V-notches and other situations such as interfaces breaking a free surface (delamination onset) cannot be correctly predicted by these two usual brittle fracture criteria. They give contradictory results and neither one nor the other agrees with the experiments [8,23]. An additional characteristic length is required to define a satisfying criterion giving rise to an approach baptised ''Finite fracture mechanics''. The crack is supposed to jump this length which depends both on the material properties and the local geometry of the structure. It is not a material parameter since the local geometry intervenes; however, it is close to the Irwin length.

The interaction between this increment and a characteristic length of the microstructure is responsible for the phenomena we consider herein.

3. Singular terms

In this section, we focus our attention on the plane elastic field at the tip, first of a sharp V-notch, and next of a blunt one. It is a generic case of stress concentration due to a singular point in the geometry of a structure.

In the vicinity of the tip (Fig. 1), in plane elasticity, the displacement field expands as [8,9,16]

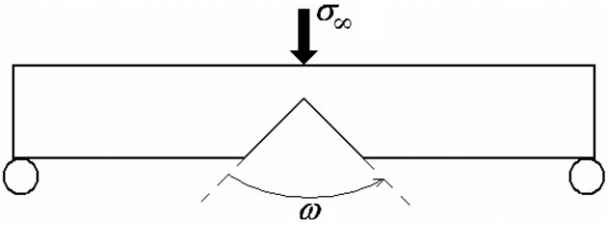

Fig. 1. Three-point bending on a V-notch specimen.

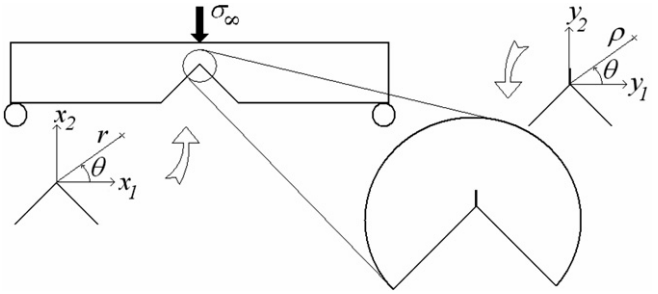

Fig. 2. The onset of a short crack at the sharp root of a V-notch.

$$\underline{U}(x_1,x_2) = \underline{U}(0,0) + kr^{\lambda}\underline{u}(\theta) + \cdots \tag{6}$$

x_1, x_2 and r,θ hold respectively for the Cartesian and polar coordinates (Cartesian and polar frames are reported in Fig. 2 and the followings). $\underline{U}(0,0)$ is the rigid translation of the origin located at the root of the notch, it plays no role and is mentioned only for consistency reasons. In general, the singularity exponent λ lies between 1/2 and 1; it can be either real or complex, single or multiple. It is associated with an angular function $\underline{u}(\theta)$; λ and $\underline{u}(\theta)$ are solutions to an eigenvalue problem. A single mode is exhibited, in the present case it is symmetric, the antisymmetric one (corresponding to a larger exponent) is not activated in a three-point bending test. The parameter k is the so-called generalized stress intensity factor (GSIF); it is proportional to the applied load σ_∞

$$k = \kappa\sigma_\infty \tag{7}$$

Note that if $\lambda < 1$ then σ is infinite at the notch tip and the inequality (5) holds true whatever the applied load. The conclusion that can be drawn from the maximum stress criterion does not match with experiments on V-notch specimens, crack initiation does occur but not for any infinitely small applied load.

As a particular case, for $\omega = 0$ ($\lambda = 1/2$) the usual opening mode I is active

$$\underline{U}(x_1,x_2) = \underline{U}(0,0) + k_I\sqrt{r}\underline{u}_I(\theta) + \cdots \tag{8}$$

The coefficient k_I is the classical mode I stress intensity factor (the GSIF for $\lambda = 1/2$) and $\underline{u}_I$ the associated opening mode.

For $\omega = \pi$ ($\lambda = 1$) there is no longer any corner non-stress concentration, the edge is straight, the elastic solution involves the non-singular T-stress (i.e. the tension parallel to the edge)

$$\underline{U}(x_1,x_2) = \underline{U}(0,0) + Tr\underline{t}(\theta) + \cdots \tag{9}$$

where the function $r\underline{t}(\theta)$ fulfils the relations $\sigma_{11} = 1, \sigma_{12} = \sigma_{22} = 0$ (The edge is in direction 1) and where T holds for the uniform tension (the GSIF for $\lambda = 1$).

4. Matched asymptotic expansions

A good knowledge of the matched asymptotic expansions procedure on the generic case of the sharp V-notch allows a better understanding of the forthcoming differences that will lead to exhibit a dependency of the apparent resistance on the actual value of a parameter characterising a microstructure size, what we call herein the size effect. Thus, in a first step the sharp V-notch problem is investigated. As seen in Fig. 2, there is no characteristic length associated to the microstructure. The size effect will intervene in the second step where a blunt V-notch with a finite root radius is considered (Fig. 3).

4.1. The sharp V-notch

Solving numerically an elasticity problem in a domain Ω^{ℓ} embedding a short crack of length ℓ at the root of the V-notch (Fig. 2) presents some difficulties because of the small size of the perturbation which requires a

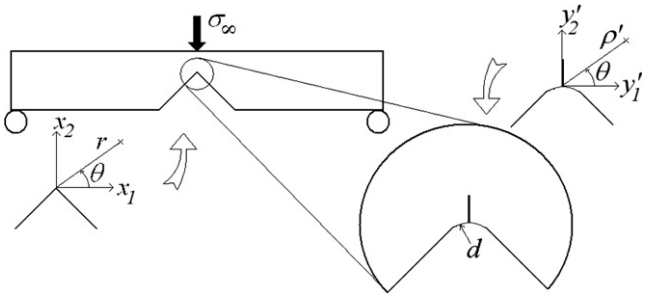

Fig. 3. The onset of a short crack at the blunted root of a V-notch.

drastic finite element (FE) mesh refinement in its vicinity for instance. It is better trying to represent the solution $\underline{U}^\ell$ in the form of an outer expansion or expansion of the far field

$$\underline{U}^\ell(x_1,x_2) = \underline{U}^0(x_1,x_2) + \text{small correction} \tag{10}$$

where $\underline{U}^0$ is solution to the same elasticity problem, but now posed on the unperturbed domain Ω^0 (Fig. 1) that can be considered as the limit of Ω^ℓ as $\ell \to 0$. In other words, the short crack is not visible. It is the classical simplified frame often used to perform FE computations, since strong mesh refinements prevent to take into account too small details.

It is clear that this solution $\underline{U}^0$ constitutes a satisfying approximation of $\underline{U}^\ell$ as one moves away from the perturbation, i.e., outside a neighbourhood of the perturbation, and thence its designation as the outer field (or far field, or remote field).

Evidently, this information is incomplete, particularly when we are interested in the fracture mechanisms. We therefore dilate the space variables by introducing the change of variables $y_i = x_i/\ell$. In the limit when $\ell \to 0$, we obtain an unbounded domain Ω^{in} (looking like the enlarge frame in Fig. 2) in which the length of the crack is now equal to 1.

We then search for a different representation of the solution under the form of an expansion known as interior field or near field

$$\underline{U}^\ell(x_1,x_2) = \underline{U}^\ell(\ell y_1,\ell y_2) = F_0(\ell)\underline{V}^0(y_1,y_2) + F_1(\ell)\underline{V}^1(y_1,y_2) + \cdots \tag{11}$$

where $F_1(\ell)/F_0(\ell) \to 0$ as $\ell \to 0$. When we substitute this expression in the equations of the problems for the determination of $\underline{V}^0$, $\underline{V}^1, \ldots$ we notice that there is a lack of the conditions at infinity to have correctly stated problems. These missing conditions will be furnished by the matching conditions.

The interior and exterior expansions describe the solution $\underline{U}^\ell$ in terms of the near field and the far field. There must be an intermediate zone (close to the perturbation for the far field and far from it for the near field) where both expansions are valid. In other words, the behaviour of the far field, when one moves closer to the origin, must match with the behaviour of the near field, when one moves away from the perturbation.

The behaviour of the far field near the origin, which is the solution of a problem posed in Ω^0, is described by the expansion in powers of r as previously encountered in Eq. (6)

$$\underline{U}^0(x_1,x_2) = \underline{U}^0(0,0) + kr^\lambda \underline{u}(\theta) + \cdots \tag{12}$$

The matching conditions can then be written as follows:

$$F_0(\ell)\underline{V}^0(y_1,y_2) \approx \underline{U}^0(0,0), \quad F_1(\ell)\underline{V}^1(y_1,y_2) \approx k\ell^\lambda \rho^\lambda \underline{u}(\theta) \tag{13}$$

when $\rho = r/\ell = \sqrt{y_1^2+y_2^2} \to \infty$ (the symbol $\approx$ means here "behaves like"), thus

$$F_0(\ell) = 1, \quad \underline{V}^0(y_1,y_2) = \underline{U}^0(0,0), \quad \text{and} \quad F_1(\ell) = k\ell^\lambda, \quad \underline{V}^1(y_1,y_2) \approx \rho^\lambda \underline{u}(\theta) \quad \text{at infinity} \tag{14}$$

Or, proceeding by superposition

$$\underline{V}^1(y_1,y_2) = \rho^\lambda \underline{u}(\theta) + \widehat{\underline{V}}^1(y_1,y_2) \quad \text{with } \widehat{\underline{V}}^1(y_1,y_2) \to 0 \quad \text{at infinity} \tag{15}$$

Then, Eq. (11) rewrites finally

$$\underline{U}^{\ell}(x_1,x_2)=\underline{U}^{\ell}(\ell y_1,\ell y_2)=\underline{U}^{0}(0,0)+k\ell^{\lambda}\underline{V}^{1}(y_1,y_2)+\cdots \tag{16}$$

Note that the matching statement in (13) is nothing else than the classical so-called remote load at infinity (see also $(19)_2$).

We now have at our disposition two descriptions of the solution $\underline{U}^{\ell}$ and in particular we can remark that, because of the derivation rule $\partial./\partial x_i=1/\ell\ \partial./\partial y_i$, the stress field associated with $\underline{U}^{\ell}$, in the neighbourhood of the perturbation, is given as a function of ℓ by

$$\underline{\underline{\sigma}}(\underline{U}^{\ell}(x_1,x_2))=k\ell^{\lambda-1}\underline{\underline{\tilde{\sigma}}}(\underline{V}^{1}(y_1,y_2))+\cdots \tag{17}$$

where the elastic constitutive law reads either

$$\underline{\underline{\sigma}}(\underline{U}^{\ell})=C:\nabla_x^S\underline{U}^{\ell}\quad\text{or}\quad\underline{\underline{\tilde{\sigma}}}(\underline{V}^{1})=C:\nabla_y^S\underline{V}^{1} \tag{18}$$

∇_x^S and ∇_y^S designate the symmetric part of the gradient operators with respect to x and y respectively, and C the elastic stiffness matrix. The term $\underline{\underline{\tilde{\sigma}}}(\underline{V}^{1})$ is independent of the global geometry of the structure as well as of the loading intensity.

The function $\underline{V}^{1}(y_1,y_2)$ is computed once for all by finite elements [8,9,16] in an artificially bounded (at a large distance of the perturbation) domain with either a Neumann or a Dirichlet condition prescribed along the new fictitious boundary Γ^{∞} (with unit outer normal $\underline{n}$)

$$\underline{V}^{1}(y_1,y_2)=\sqrt{\rho}\underline{u}_I(\theta)\ \text{(Dirichlet)}\quad\text{or}\quad\underline{\underline{\tilde{\sigma}}}(\underline{V}^{1})\cdot\underline{n}=\underline{\underline{\tilde{\sigma}}}(\sqrt{\rho}\underline{u}_I(\theta))\cdot\underline{n}\ \text{(Neumann)} \tag{19}$$

The change in potential energy due to the crack onset can be expressed by mean of a path independent integral Ψ [16,23]

$$-\delta W_{\mathrm{p}}=\Psi(\underline{U}^{\ell},\underline{U}^{0}) \tag{20}$$

with

$$\Psi(\underline{U}^{\ell},\underline{U}^{0})=\frac{1}{2}\int_{\Gamma}\left[\underline{\underline{\sigma}}(\underline{U}^{\ell})\cdot\underline{N}\cdot\underline{U}^{0}-\underline{\underline{\sigma}}(\underline{U}^{0})\cdot\underline{N}\cdot\underline{U}^{\ell}\right]\mathrm{d}s \tag{21}$$

where Γ is any closed contour surrounding the corner and the crack extension starting and finishing on the two stress free faces of the wedge and $\underline{N}$ a unit normal to the line Γ pointing toward the root of the corner. It is computed in Ω^{in} with the appropriate change of variables.

Then replacing the above expansions, once for $\ell=0$ and once for $\ell\neq 0$, into (20) leads to

$$-\delta W_{\mathrm{p}}=k^2\ell^{2\lambda}Ae+\cdots \tag{22}$$

In (22), e holds for the specimen thickness (plane elasticity) and A is a geometrical coefficient depending only on the V-notch opening ω. It is extracted from $\underline{V}^{1}$ using the path independent integral Ψ

$$A=\Psi(\underline{V}^{1}(y_1,y_2),\rho^{\lambda}\underline{u}(\theta)) \tag{23}$$

The energy condition resulting from (22) writes

$$G_{\mathrm{i}}=-\frac{\delta W_{\mathrm{p}}}{\delta S}=-\frac{\delta W_{\mathrm{p}}}{\ell e}=k^2\ell^{2\lambda-1}A\geqslant G_{\mathrm{c}} \tag{24}$$

It is clear that if $\lambda>1/2$ then $G_d=\lim_{\ell\to 0}G_{\mathrm{i}}=0$ (see Eqs. (3) and (4)) and the above inequality can never be fulfilled. As already reported, the Griffith criterion addresses only the continuous growth of pre-existing cracks ($\lambda=1/2$).

It can be noted that the knowledge of $k_{I\mathrm{c}}$ instead of G_{c} avoids the use of the elastic constants (see Eq. (2)), thus the computation of $\underline{V}^{1}$ can be carried out once for all for $E=1$.

Following [8], the stress condition must hold true all along the putative crack path of length ℓ:

$$\sigma_{\theta\theta}(\ell)\geqslant\sigma_{\mathrm{c}} \tag{25}$$

where $\sigma_{\theta\theta}(\ell)$ is the hoop stress measured at the distance ℓ from the notch root along the bisector (the crack direction because of the symmetry) prior to any crack initiation. It is a decreasing function of ℓ. According

to the various expansions and an appropriate normalization of the eigenvector $\underline{u}(\theta)$ [8,9], at the leading order, the inequality (25) writes

$$k\ell^{\lambda-1} \geqslant \sigma_c \tag{26}$$

since in that case (i.e. prior to crack initiation) $\widehat{\underline{V}}^1 = 0$ (see Eq. (15)).

The crack initiation length ℓ_0 must fulfil the two inequalities (24) and (26) and thus depends only on the V-notch opening

$$\ell_0 = \frac{G_c}{A\sigma_c^2} \tag{27}$$

The resulting Irwin-like failure initiation criterion reads [8]

$$k \geqslant k_c = \left(\frac{G_c}{A}\right)^{1-\lambda} \sigma_c^{2\lambda-1} \tag{28}$$

The critical value k_c depends only on the failure parameters of the material and on the V-notch opening. It coincides with the Griffith's criterion (in the Irwin's form) for a crack ($\lambda = 1/2$) and with the stress criterion for a straight edge ($\lambda = 1$). Moreover, according to (7), the above criterion (28) rewrites

$$\sigma_\infty \geqslant \frac{1}{\kappa}\left(\frac{G_c}{A}\right)^{1-\lambda} \sigma_c^{2\lambda-1} \tag{29}$$

The applied load at failure does not depend on any representative length of a microstructure; there is no size effect in this step.

Remark: The contour integral Ψ can be used also to compute the GSIF k

$$k = \frac{\Psi(\underline{U}^0, r^{-\lambda}\underline{u}^-(\theta))}{\Psi(r^\lambda \underline{u}(\theta), r^{-\lambda}\underline{u}^-(\theta))} \tag{30}$$

where $r^{-\lambda}\underline{u}^-(\theta)$ is the dual function to the singular mode $r^\lambda \underline{u}(\theta)$ [16,23].

4.1.1. The blunted V-notch

In a second step, we still consider a short crack of length ℓ but the V-notch is now blunted and there is a small notch root radius d (Fig. 3), the crack length ℓ is assumed to be smaller or of the same order of magnitude than d.

If d is small, it is clear that the far field or outer expansion remains unchanged at the leading order (Eqs. (6) and (10)), details are still not visible. But there is now a choice to do for the dilation that can be performed either with respect to ℓ or to d. Both cases must lead to identical results but it is easier to use d for practical reasons (FE meshes). Then the stretched domain exhibits a notch root radius equal to 1 and a crack of dimensionless length $\mu = \ell/d$.

The inner expansion now writes

$$\underline{U}^{\ell,d}(x_1, x_2) = \underline{U}^{\ell,d}(\mathrm{d}y_1', \mathrm{d}y_2') = H_0(d)\underline{W}^0(y_1', y_2', \mu) + H_1(d)\underline{W}^1(y_1', y_2', \mu) + \cdots \tag{31}$$

where $y_i' = x_i/d$ and $H_1(d)/H_0(d) \to 0$ as $d \to 0$. The dependence of the different terms $\underline{W}^0$, $\underline{W}^1$ on the stretched crack length μ is highlighted. The matching conditions lead to

$$H_0(d) = 1, \underline{W}^0(y_1', y_2', \mu) = \underline{U}^0(0,0), \quad \text{and} \quad H_1(d) = kd^\lambda, \underline{W}^1(y_1', y_2', \mu) \approx \rho'^\lambda \underline{u}(\theta) \text{ at infinity} \tag{32}$$

with $\rho' = r/d = \sqrt{y_1'^2 + y_2'^2}$. The change in potential energy and the resulting energy condition now write

$$-\delta W_p = k^2 d^{2\lambda}(B(\mu) - B(0))e = k^2 \ell^{2\lambda} \frac{B(\mu) - B(0)}{\mu^{2\lambda}} e \tag{33}$$

$$G_i = -\frac{\delta W_p}{\ell e} = k^2 d^{2\lambda-1} \frac{B(\mu) - B(0)}{\mu} = k^2 \ell^{2\lambda-1} \frac{B(\mu) - B(0)}{\mu^{2\lambda}} \geqslant G_c \tag{34}$$

The function $B(\mu)$ is extracted from $\underline{W}^1(y_1', y_2', \mu)$ computed by finite elements for each μ using the Ψ integral (see Eqs. (21) and (23) above), it is independent of the global geometry and the applied load

$$B(\mu) = \Psi(\underline{V}^1(y_1', y_2', \mu), \rho^\lambda \underline{u}(\theta)) \tag{35}$$

Now the energy condition depends not only on the V-notch opening ω and the crack length ℓ, as in inequality (24), but also on the local geometry through the dimensionless parameter μ.

The stress condition stated prior to any crack initiation (i.e. using Eq. (14) for $\underline{W}^1$ with $\mu = 0$), writes

$$kd^{\lambda-1}\tilde{\sigma}_{\theta\theta}(\underline{W}^1(y_1', y_2', 0))\big|_{\sqrt{y_1'^2+y_2'^2}=\mu} \geqslant \sigma_c \tag{36}$$

where the hoop stress $\tilde{\sigma}_{\theta\theta}$ is computed at the distance $\sqrt{y_1'^2 + y_2'^2} = \mu$ in the dilated domain. Once again, the two inequalities (34) and (36) can be solved, implicitly here (see the example in Section 6), to provide the crack initiation length $\ell_0 = \mu_0 d$. It fulfils the non-linear equation

$$\frac{1}{\left(\tilde{\sigma}_{\theta\theta}(\underline{W}^1(y_1', y_2', 0))\big|_{\sqrt{y_1'^2+y_2'^2}=\mu_0}\right)^2} \frac{B(\mu_0) - B(0)}{\mu_0} = \frac{1}{d}\frac{G_c}{\sigma_c^2} \tag{37}$$

The initiation criterion (34), with $\ell = \ell_0$, involves the GSIF k extracted from the far field which does not depend on any micro structure size, while the critical value k_c^{app} does through μ_0

$$k \geqslant k_c^{\text{app}} = \left(\frac{G_c}{D(\mu_0)}\right)^{1-\lambda} \left(\frac{\sigma_c}{\tilde{\sigma}_{\theta\theta}(\underline{W}^1(y_1', y_2', 0))\big|_{\sqrt{y_1'^2+y_2'^2}=\mu_0}}\right)^{2\lambda-1} \quad \text{with } D(\mu_0) = \frac{B(\mu_0) - B(0)}{\mu_0} \tag{38}$$

As a consequence there is now a size effect, according to (7), the remote load at failure is a function of the actual microstructure length d through $\mu_0 = \ell_0/d$ since it fulfils

$$\sigma_\infty \geqslant \frac{1}{\kappa}\left(\frac{G_c}{D(\mu_0)}\right)^{1-\lambda} \left(\frac{\sigma_c}{\tilde{\sigma}_{\theta\theta}(\underline{W}^1(y_1', y_2', 0))\big|_{\sqrt{y_1'^2+y_2'^2}=\mu_0}}\right)^{2\lambda-1} \tag{39}$$

It proves useful to compare the above relationship, including a size effect, with (29), which is free of size effects. A practical parameter to quantify this effect is the ratio

$$R = \frac{k_c^{\text{app}}}{k_c} = \left(\frac{A}{D(\mu_0)}\right)^{1-\lambda} \left(\frac{1}{\tilde{\sigma}_{\theta\theta}(\underline{W}^1(y_1', y_2', 0))\big|_{\sqrt{y_1'^2+y_2'^2}=\mu_0}}\right)^{2\lambda-1} \tag{40}$$

$R > 1$ (resp. $R < 1$) expresses a strengthening (resp. weakening) phenomenon.

The criterion (38) or (39), as well as the parameter R, are independent of any macroscopic length able to characterize the specimens or structures size. Thus any analysis of homothetic specimens or structures is irrelevant here. The meaningful quantity is the actual value of the small parameter d, characteristic of the geometry at the microscale.

Relations (38)–(40) are valid in many different situations as illustrated in the following examples of Sections 5–8.

5. Example 1: failure at a blunted notch

5.1. The V-notched specimens in bending

In [9], the above analysis was performed in the generic case of a blunted V-notch (Fig. 3) and a comparison is made with three-point bending experiments by Dunn et al. [24] on PMMA ($E = 2.3$ GPa, $\nu = 0.36$, $G_c = 394$ J m^{-2}, $\sigma_c = 124$ MPa, specimens size: length 76.2 mm × width 17.8 mm × thickness 12.7 mm). Fig. 4 shows the apparent toughness improvement brought by the notch root radius d (ranging from 1 to

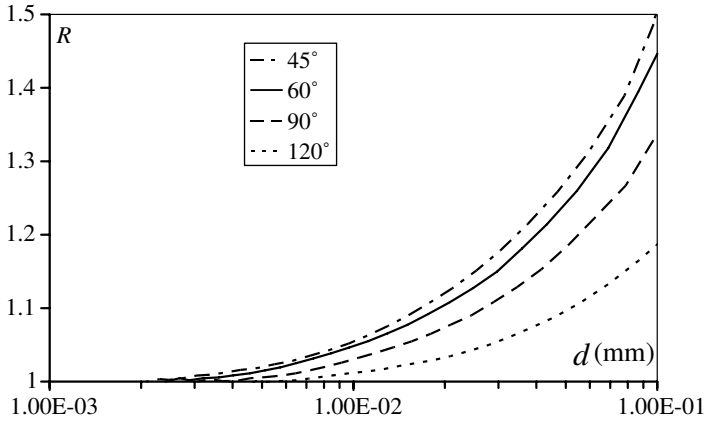

Fig. 4. The apparent toughness improvement R brought by the notch root radius d (mm) for different V-notch opening [9].

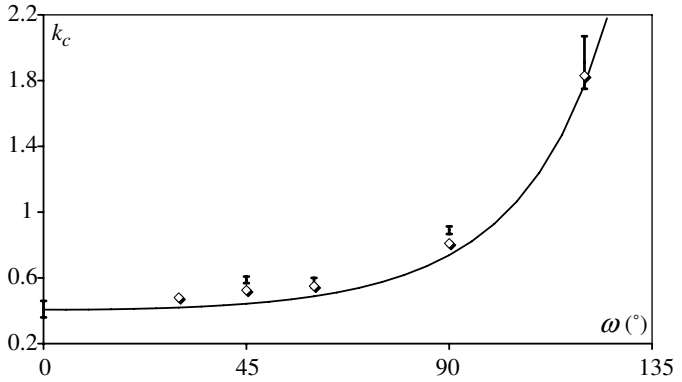

Fig. 5. Comparison with experiments by Dunn et al. on PMMA specimens (all results are from Dunn et al. [24] except $\omega = 45°$ from Yosibash et al. [25]). (1) Experiments (error bars), (2) Prediction using the sharp notch criterion (solid line), (3) Correction for a notch tip radius $d = 25.4$ μm ($d = 30$ μm for $\omega = 45°$) (diamonds). From [9].

100 μm) for different openings ω. Along the vertical axis is the ratio R (40) of the apparent GSIF k_c^{app} to the primary GSIF k. In Fig. 5, the criterion corresponding to a sharp notch (solid line) is compared to the corrected one (diamonds) taking into account a small notch root radius as reported in the experiments by Dunn et al. [24] and Yosibash et al. [25].

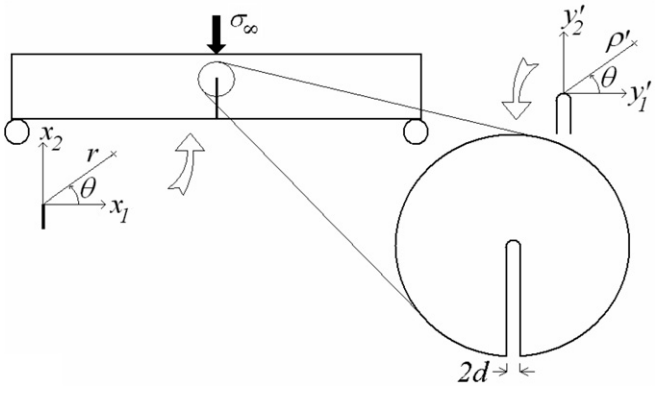

Fig. 6. A blunt notch in a three-point bending specimen.

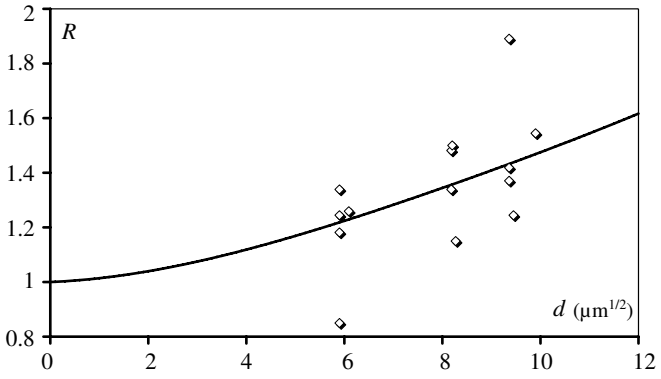

Fig. 7. The ratio R vs. the square root of the notch-root radius $\sqrt{d}$ ($\mu m^{1/2}$) for Silicon Nitride. (1) experiments (diamonds) [26] and (2) prediction (solid line).

5.1.1. The single edge notched specimens in bending (SENB)

A very similar study has been carried out on notched specimens of ceramics. The measure of the toughness in ceramic materials is performed using three-point bending on so-called SENB specimens (Fig. 6). Nevertheless it is very difficult or impossible to machine a perfect sharp slit; there is necessarily a rounded tip and the toughness measure is biased [26]. In [10] the authors propose a correction to bring to the measure in terms of the root radius d. In that case the far field problem is the usual three-point bending cracked specimen and involves the classical mode I stress intensity factor k_I. Corrections are illustrated in Fig. 7 dedicated to Silicon Nitride ($\sigma_c = 580$ MPa, $k_{Ic} = 5.4$ MPa $m^{1/2}$, specimens size: $45 \times 4 \times 3$ mm) and showing the ratio R of the apparent (measured) toughness k_{Ic}^{app} to the actual toughness k_{Ic} as a function of the square root of the blunting radius $\sqrt{d}$ (used classically as a relevant parameter in this kind of experiments and models).

6. Example 2: the step-over mechanism

As a second example, let us consider a case frequently observed in bedded sediments (and in layered ceramics by the way). A primary crack impinges on an interlayer (Fig. 8) and there is a competition between the crack growth through the interlayer and a step-over the interlayer with a new crack onset in the next bed of sediments. This problem is of great interest for the oil and gas industry, a better understanding of this kind of mechanisms will surely lead to a better characterization of fractured reservoirs and to an improvement of the predictive models of oil and gas production.

In the simplified frame of Fig. 8, the structure is submitted to a remote tension σ_∞. The pre-existing crack is therefore undergoing a mode I opening. Attention is paid to bring out the size effect resulting from variations of the interlayer thickness d.

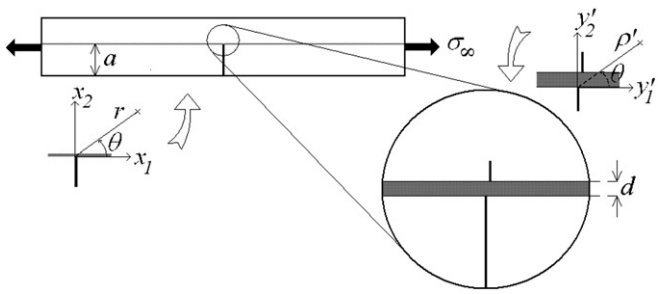

Fig. 8. A crack impinging on an interlayer and the step-over mechanism.

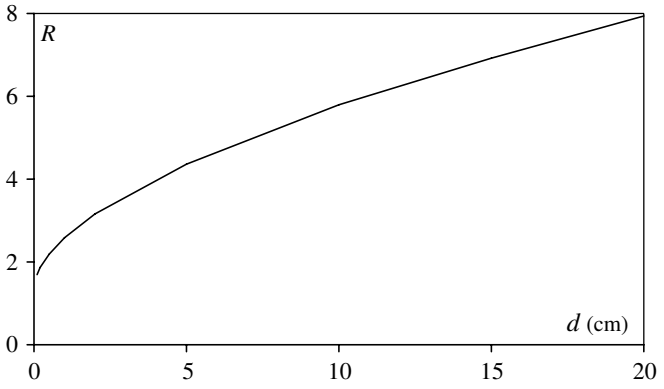

Fig. 9. The ratio R for the step-over mechanism vs. the thickness d (cm) of the shale interlayer.

As already mentioned the far field is obtained for $d \to 0$, then the interlayer disappears and the far field involves the classical crack tip stress intensity factor k_I. It is related to the remote tension according to Tada's formula (a is the thickness of the adjacent beds, Fig. 8)

$$k_I = 5\sigma_\infty a^{1/2} \tag{41}$$

The final form of the criterion is still (38) with $\lambda = 0.5$. In the following numerical example, the two beds are made of sandstone with the material parameters: $E_1 = 2$ GPa, $\nu_1 = 0.3$, $\sigma_c = 3$ MPa, $G_c = 80$ J m^{-2}. The interlayer is made of shale with: $E_2 = 0.4$ GPa and $\nu_2 = 0.3$ (no special attention is paid to the Poisson's ratios whose values play a minor role within a reasonable range). In general situations, the sandstone beds thickness is some metres while the shale interlayers thickness is only some centimetres.

Fig. 9 shows the size effect observed on the ratio R for different shale interlayer thicknesses (in cm). It is clear that, even for very thin layers, the primary crack is strongly blunted by the soft layer of shale. As a consequence of (41), for a fixed a, the same effect is observed on the remote load

$$\sigma_\infty = \frac{Rk_{Ic}}{5a^{1/2}} \tag{42}$$

A more detailed analysis is proposed in [11] where the competition between step-over, primary crack arrest and penetration in the shale layer is studied in response to a remote horizontal tension and a vertical overburden compression (prohibiting any horizontal crack deflection along the interlayer). Moreover, it must be noted that this step-over mechanism is accompanied by a slight shift (ignored herein), the new crack is not strictly ahead of the primary one but a little aside.

7. Example 3: failure in tension at a hole in a PMMA specimen

Let us consider a small circular hole in a plate of PMMA submitted to a remote tension σ_∞ (Fig. 10). The drilled plate is assumed to be sufficiently thick to promote a plane strain analysis rather than a plane stress one. The cavity diameter d is assumed to be small compared to the plate length or width. The two small parameters are the crack increment length and the diameter of the hole. In this case there is a stress concentration but no singularity. Nevertheless, the reasoning remains the same, the leading term of the far field expansion ($d \to 0$) reduces to a single term

$$\underline{U}^0(x_1, x_2) = \sigma_\infty r\underline{t}(\theta) \tag{43}$$

The function $r\underline{t}(\theta)$ is similar to that in equation (9).

The inner problem prior to any crack onset is an infinite plate with a hole of diameter 1 submitted to a remote tension σ_∞ at infinity. In this case the solution $\underline{W}^1(y_1', y_2', 0)$ is known analytically [27] and the tension on both sides of the hole (at the "equator") at a distance ℓ such that $\ell = \mu d$, prior to any crack onset writes at the leading order

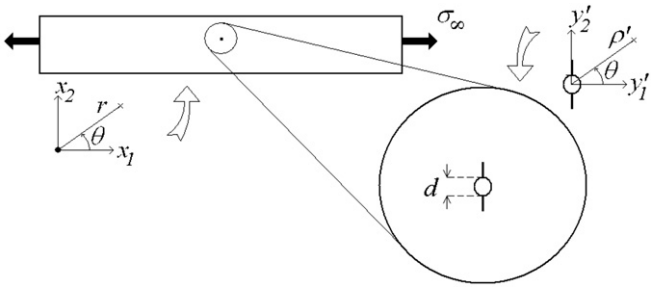

Fig. 10. A circular hole in a PMMA plate in tension with two short cracks at the "equator".

$$\sigma = \sigma_\infty + \frac{\sigma_\infty}{2}\left[\left(\frac{1}{2\mu+1}\right)^2 + 3\left(\frac{1}{2\mu+1}\right)^4\right] = \sigma_\infty \tilde{\sigma}(\mu) \tag{44}$$

Clearly, the stress concentration factor of such geometry is 3; $\sigma = 3\sigma_\infty$ at $\mu = 0$, i.e. on the two sides of the hole. Following a maximum stress criterion, failure would occur for $\sigma_\infty = \sigma_c/3$ whatever the diameter of the cavity. It is contradictory with the experiments showing that if the cavity size becomes smaller then the applied load leading to failure increases from $\sigma_c/3$ to σ_c [15].

The energy condition (34) together with Eq. (44) and the stress condition $\sigma = \sigma_c$ lead to the equation defining the crack initiation length $\ell_0 = \mu_0 d$ (keep in mind that there are two symmetric cracks with a total length $2\ell_0$ as shown in Fig. 10) solution to the equation (the analogous to (37))

$$\frac{1}{\tilde{\sigma}^2(\mu_0)} \cdot \frac{B(\mu_0) - B(0)}{2\mu_0} = \frac{1}{d}\frac{G_c}{\sigma_c^2} \tag{45}$$

As already reported, the function $B(\mu)$ is extracted from $\underline{\underline{W}}^1(y_1', y_2', \mu)$ computed by finite elements. Replacing now μ_0 in Eq. (44) with in addition the stress condition $\sigma = \sigma_c$ finally allows determining σ_∞ at failure as illustrated in Fig. 11.

$$\sigma_\infty = \frac{\sigma_c}{\tilde{\sigma}(\mu_0)} \tag{46}$$

The solid line is the theoretical prediction and the diamonds correspond to experiments on PMMA [20] ($E = 3$ GPa, $\nu = 0.36$, $G_c = 290$ J m^{-2}, $\sigma_c = 72$ MPa, specimens size: $100 \times 30 \times 10$ mm). Clearly this approach is able to render the size effect observed in the experiments (Fig. 5) not as perfectly as expected, new experiments are still in progress. It can be noted that Li and Zhang [20] propose to improve the present criterion

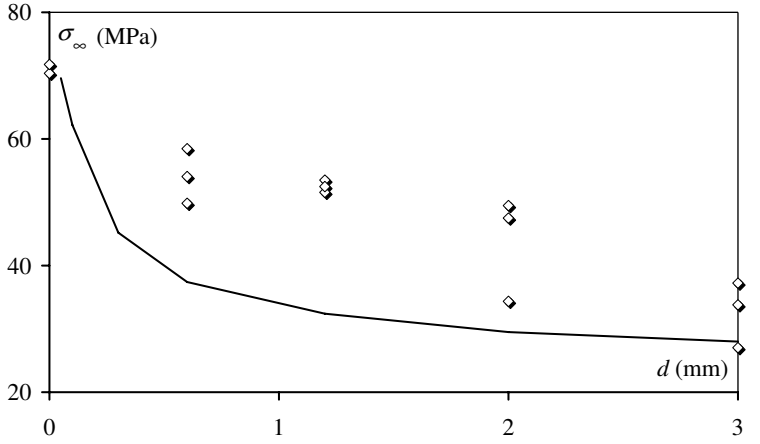

Fig. 11. Failure load prediction (solid line) compared to experiments [20] (diamonds).

using an additional parameter taking into account the quasi-brittleness of PMMA and the roughness of the fracture pattern.

8. Example 4: failure in compression in rocks

Let us consider again a circular hole in a specimen of rock but submitted now to a remote compressive load σ_∞ (Fig. 12). As in the first example, the two small parameters are the crack increment length ℓ and the diameter d of the hole.

The far field is unchanged and still reduces to a single term (Eq. (43)) but with $\sigma_\infty < 0$. As above, the inner field is known analytically and the tension at a distance ℓ such that $\ell = \mu d$ along the axis passing through the two poles of the cavity writes [27]

$$\sigma = \frac{\sigma_\infty}{2}\left[\left(\frac{1}{2\mu+1}\right)^2 - 3\left(\frac{1}{2\mu+1}\right)^4\right] \tag{47}$$

The tension at the two poles, i.e. at $\mu = 0$ is then $\sigma = -\sigma_\infty$. The use of the stress criterion would lead to the prediction of cracks initiation at the two poles if $\sigma_\infty = -\sigma_c$, conclusion that is in general contradictory with the experiments [21,22]. It is almost true if the hole is sufficiently large (although remaining small compared to the specimen); but the compression must be increased as the hole diameter decreases. The strength in compression is of course an upper bound to this loading process.

The method described above to derive numerically the load initiating the fracture mechanism for the plate under tensile load, and especially the Eq. (45), remains the same for compressive conditions. Now σ_∞ has a negative value, $\tilde{\sigma}$ is computed along the axis passing through the two poles and the function still noted B corresponds to the concerned perturbation, i.e. two cracks at the poles instead of two cracks at the equator.

This case has been investigated by different authors [17,18,21]. It is experimentally convenient since the crack growth is stable but tests are difficult to carry out for practical reasons and experimental data are quite scarce in the literature. As already mentioned, usual fracture mechanics models need an initial crack length to work properly, that is sometimes taken equal to the Irwin's length. According to Sammis and Ashby's model [17] and Carter's experiment [21,22], these values of the critical crack length are usually too large to be realistic. Therefore they use the initial crack length, as well as k_{Ic}, as fitting parameters of the models. It is important to notice that in contrast to Carter's analysis, the model developed herein allows an effective numerical determination of the crack length at initiation instead of a more or less arbitrary choice.

The present theoretical predictions are compared to experimental data obtained by Carter et al. [22], on Tyndallstone (a kind of limestone) and potash rock specimens (the specimens size ranges from $152 \times 89 \times 84$ mm to $305 \times 305 \times 89$ mm [21]). For Tyndallstone, Carter et al. report values of σ_c ranging from 0.5 to 5 MPa and a value of the toughness k_{Ic} of 1 MPa $m^{1/2}$ (however measured on a sample of stronger Tyndallstone). For potash rock, the experimental tensile strength and toughness (average values) measured by Carter are $\sigma_c = 1.7$ MPa and $k_{Ic} = 0.34$ MPa $m^{1/2}$.

Figs. 13 and 14 give a comparison between computations and Carter's experimental data, represented by diamonds. The solid line gives the best agreement to the data and is obtained by implementing in the

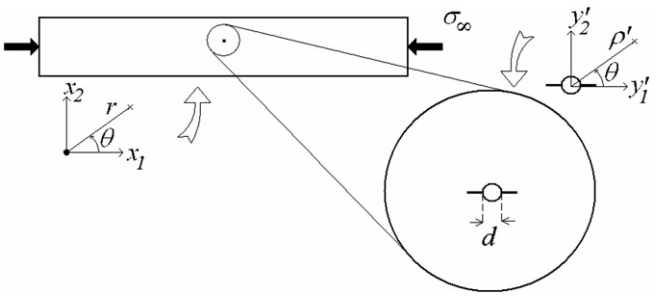

Fig. 12. A circular hole with two short cracks at the "poles" in a block under compressive load.

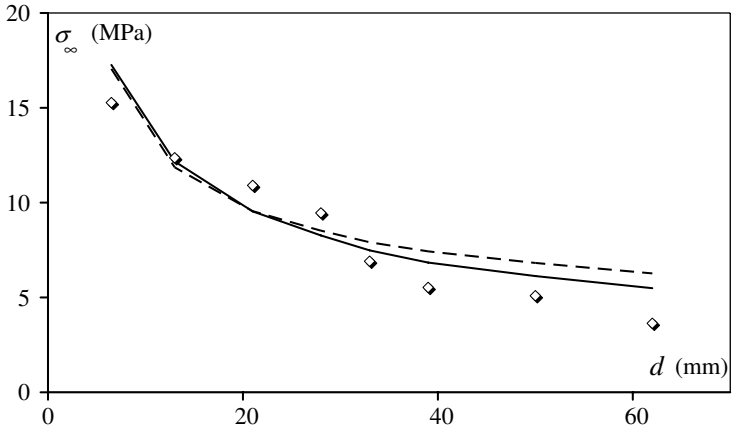

Fig. 13. Comparison between predictions (solid and dashed lines) and Carter's experimental data (diamonds) on Tyndallstone. Solid and dashed lines correspond to different tensile strength.

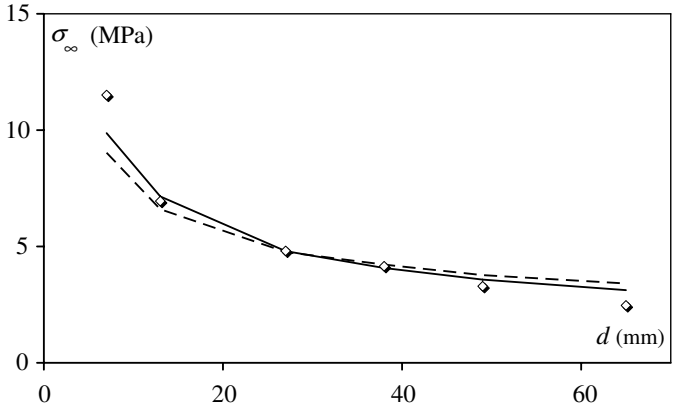

Fig. 14. Comparison between predictions (solid and dashed lines) and Carter's experimental data (diamonds) on potash rock. Solid and dashed lines correspond to different tensile strength.

computations $k_{Ic} = 0.4$ MPa $m^{1/2}$, $\sigma_c = 1.5$ MPa for Tyndallstone, and $k_{Ic} = 0.23$ MPa $m^{1/2}$, $\sigma_c = 0.4$ MPa for potash rock. The dashed lines are obtained by using $k_{Ic} = 0.4$ MPa $m^{1/2}$, $\sigma_c = 3$ MPa for Tyndallstone and $k_{Ic} = 0.22$ MPa $m^{1/2}$, $\sigma_c = 1.7$ MPa for potash rock, which are the values used by Carter to achieve his fitting process (following Sammis and Ashby's model [17]) to the experimental data. Note that these values are quite different from the measured values. All the computations are carried out with $\nu = 0.3$, once again the Poisson's ratio has not much influence on the failure computations.

The agreement is quite satisfactory. However, it is important to notice that, since the Eq. (44) depends on $1/d$, the model cannot predict a finite value of σ_∞ as d tends towards 0. But one must remind that, in all these experiments, the strength in compression is of course an upper bound of the admissible remote loads, beyond which a complete ruin of the specimen is expected. This upper bound cannot be represented here, being out of the limits of the graph (the compressive strength is ranging respectively between 40 and 70 MPa for Tyndallstone, and averages 24.5 MPa for potash rock in Carter's specimens).

For a hole in an infinite plate, Sammis and Ashby [17] found a dimensionless constant crack length μ_0 of 0.2, which is in good agreement with their experiments carried out on PMMA. With the model developed in this paper, μ_0 is found to be increasing with the size of the hole and ranges from 0.13 to 0.24 for Tyndallstone and from 0.20 to 0.29 for potash rock.

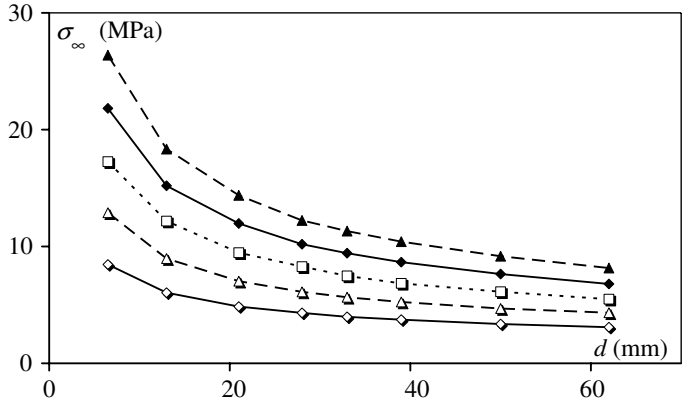

Fig. 15. Sensitivity of the model to the toughness: $k_{Ic} = 0.2$ MPa m$^{1/2}$ (diamonds, solid line), $k_{Ic} = 0.3$ MPa m$^{1/2}$ (triangles, dashed line), $k_{Ic} = 0.4$ MPa m$^{1/2}$ (squares, dotted line), $k_{Ic} = 0.5$ MPa m$^{1/2}$ (solid diamonds, solid line), $k_{Ic} = 0.6$ MPa m$^{1/2}$ (solid triangles, dashed line), for Tyndallstone.

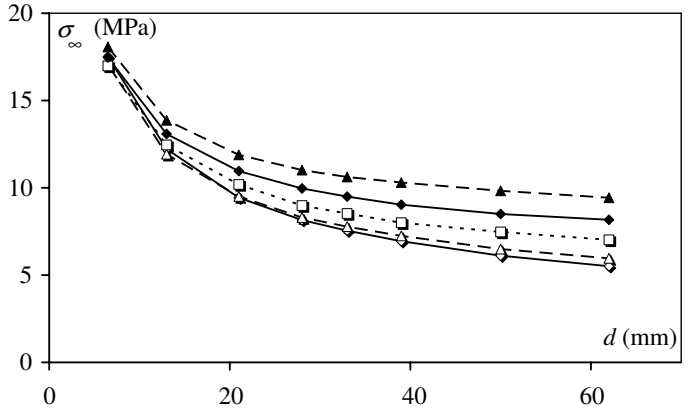

Fig. 16. Sensitivity of the model to the tensile strength: $\sigma_c = 1$ MPa (diamonds, solid line), $\sigma_c = 2.5$ MPa (triangles, dashed line), $\sigma_c = 4$ MPa (squares, dotted line), $\sigma_c = 5.5$ MPa (solid diamonds, solid line), $\sigma_c = 7$ MPa (solid triangles, dashed line), for Tyndallstone.

To better illustrate the sensitivity of the model to the failure parameters k_{Ic} and σ_c, computations have been carried out with varying values. The comparison with respect to k_{Ic} is carried out at constant $\sigma_c = 1.5$ MPa. The sensitivity analysis with respect to σ_c is carried out at constant $k_{Ic} = 0.4$ MPa m$^{1/2}$ (Figs. 15 and 16).

An increase in k_{Ic} induces an increase in both the curvature and the vertical location of the curve. This effect is more pronounced for cavities of small diameters. Increases in σ_c lead to the same changes in the curves, but discrepancies now appear for cavities of large diameters. Roughly speaking, the energy criterion takes precedence on the strength criterion for small size holes, whereas for large size holes, the strength criterion is predominant.

9. Conclusions

The matched asymptotic expansions framework allows analyzing the interaction between the length of a crack jump at initiation and a characteristic size of the microstructure. Thanks to a fracture criterion that requires fulfilling both energy and stress conditions, the equations governing the size effects have been brought into evidence and illustrated in very different situations for various brittle materials (PMMA, ceramics, rocks) and in particular in the case of holed specimens in tension and compression. In the whole set of examples, it must be pointed out that the relevant parameter is the actual root radius for blunted notches, the actual hole

diameter for cavities or the actual interlayer thickness for bedded sediments. It must be expressed using units (say μm, mm or m) and does not allow any dimensionless analysis. Homothetic specimens are irrelevant herein since the size of the specimens or of the structures has never been involved throughout the analysis, it holds true whatever the size of the structure under consideration and thus the statistical effects are not addressed.

References

[1] Weibull W. A statistical theory of the strength of materials. Proc Royal Swedish Acad of Engng Sci 1939;151:1–45.
[2] Bazant ZP. Size effect in blunt fracture: concrete, rock, metal. J Engng Mech 1984;110(4):518–35.
[3] Bazant ZP. Size effect in compression fracture: splitting crack band propagation. J Engng Mech 1997;123(2):162–72.
[4] Bazant ZP, Planas J. Fracture and size effect in concrete and other quasibrittle materials. Boca Raton: CRC Press; 1998.
[5] Hashin Z. Finite Thermoelastic Fracture Criterion with Application to Laminate Cracking Analysis. J Mech Phys Solids 1996;44:1129–45.
[6] Nairn JA. Exact and variational theorems for fracture mechanics of composites with residual stresses, traction-loaded cracks and imperfect interfaces. Int J Fract 2000;105:243–71.
[7] Taylor D, Cornetti P, Pugno N. The fracture mechanics of finite crack extension. Engng Fract Mech 2005;72(7):1021–38.
[8] Leguillon D. Strength or toughness? A criterion for crack onset at a notch. Eur J Mech A/Solids 2002;21:61–72.
[9] Leguillon D, Yosibash Z. Crack onset at a V-notch. Influence of the notch tip radius. Int J Fract 2003;122:1–21.
[10] Picard D, Leguillon D, Putot C. A method to estimate the influence of the notch-root radius on the fracture toughness of ceramics. J Eur Ceram Soc 2006;26:1421–7.
[11] Picard D. Modèle de représentation mécanique de la formation de fractures naturelles d'un réservoir pétrolier. PhD. thesis, University Pierre et Marie Curie, Paris 2005.
[12] Leguillon D, Laurencin J, Dupeux M. Failure of an epoxy joint between two steel plates. Eur J Mech A/Solids 2003;22:509–24.
[13] Leguillon D, Tariolle S, Martin E, Chartier T, Besson JL. Prediction of crack deflection in porous/dense ceramic laminates. J Eur Ceram Soc 2006;26:343–9.
[14] Leguillon D, Lacroix C, Martin E. Interface debonding ahead of a primary crack. J Mech Phys Solids 2000;48:2137–61.
[15] Martin E, Leguillon D. Energetic conditions for interfacial failure in the vicinity of a matrix crack in brittle matrix composites. Int J Solids Struct 2004;41:6937–48.
[16] Leguillon D, Sanchez-Palencia E. Computation of singular solutions in elliptic problems and elasticity, Masson, Paris, J. Wiley, New York 1987.
[17] Sammis CG, Ashby MF. The failure of brittle porous solids under compressive stress states. Acta Metall 1986;34(3):511–26.
[18] He MY, Turner MR, Evans AG. Analysis of the double cleavage drilled compression specimen for interface fracture energy measurements over a range of mode mixities. Acta Metal Mater 1995;43(9):3453–8.
[19] Wong RHC, Lin P, Tang CA. Experimental and numerical study on splitting failure of brittle solids containing single pore under uniaxial compression. Mech Mat 2006;38:142–59.
[20] Li J, Zhang XB. A criterion study for non-singular stress concentrations in brittle or quasi brittle materials. Engng Fract Mech 2006;73:503–23.
[21] Carter BJ. Size and stress gradient effects on fracture around cavities. Rock Mech Rock Engng 1992;25(3):167–86.
[22] Carter BJ, Lajtai EZ, Yanguang Y. Tensile fracture from circular cavities loaded in compression. Int J Fract 1992;57:221–36.
[23] Labossiere PEW, Dunn ML. Stress intensities at interface corners in anisotropic bimaterials. Engng Fracture Mech 1999;62:555–75.
[24] Dunn ML, Suwito W, Cunningham S. Fracture initiation at sharp notches: correlation using critical stress intensities. Int J Solids Struct 1997;34(29):3873–84.
[25] Yosibash Z, Bussiba A, Gilad I. Failure criteria for brittle elastic materials. Int J Fract 2004;125(3-4):307–33.
[26] Damani R, Gstrein R, Danzer R. Critical notch-root radius effect in SENB-S fracture toughness testing. J Eur Ceram Soc 1996;16:695–702.
[27] Timoshenko SP, Goodier JN. Theory of elasticity. 3rd ed. New York: Mc Graw Hill; 1970.